Identification of vacancy defects in compound semiconductors by core-electron annihilation: Application to InP — Source link ⧉

Matti Alatalo, H. Kauppinen, Kimmo Saarinen, Martti J. Puska ...+3 more authors

Related papers:

- Increased Elemental Specificity of Positron Annihilation Spectra.

- Theoretical and experimental study of positron annihilation with core electrons in solids

- Theory of Positrons in Solids and on Solid Surfaces

- Positron-annihilation momentum profiles in aluminum: Core contribution and the independent-particle model

- Defect identification using the core-electron contribution in Doppler-broadening spectroscopy of positron-annihilation radiation.

Alatalo, M.; Kauppinen, H.; Saarinen, K.; Puska, M.J.; Mäkinen, J.; Hautojärvi, P.; Nieminen, R.M.

Identification of vacancy defects in compound semiconductors by core-electron annihilation: Application to InP

Identification of vacancy defects in compound semiconductors by core-electron annihilation: Application to InP

M. Alatalo, H. Kauppinen, K. Saarinen, M. J. Puska, J. Mäkinen, P. Hautojärvi, and
R. M. Nieminen

Laboratory of Physics, Helsinki University of Technology, FIN-02150 Espoo, Finland

(Received 21 June 1994)

We show that the Doppler broadening of positron annihilation radiation can be used in the identification of vacancy defects in compound semiconductors. Annihilation of trapped positrons with surrounding core electrons reveals chemical information that becomes visible when the experimental background is reduced by the coincidence technique. We also present a simple calculational scheme to predict the high-momentum part of the annihilation line. The utility of the method is demonstrated by providing results for vacancies in InP. In electron irradiated InP the isolated In and P vacancies are distinguished from each other by the magnitude of the core electron annihilation. In heavily Zn-doped InP we detect a native vacancy defect and identify it to a P vacancy decorated by Zn atoms.

I. INTRODUCTION

Positron annihilation spectroscopy has turned out to be a powerful technique to study vacancy defects in semiconductors.[1] A vacancy defect acts as a positron trap. The trapped positron lifetime is proportional to the open volume of the defect,[2] and, therefore, single and multiple vacancies can be identified. It is also possible to distinguish between different charge states of vacancies based on changes in positron lifetime or trapping rate.[3,4]

Comparing the observed changes in the lifetimes with the results of the recent first principles calculations[5–7] for the atomic relaxations helps to understand the configurations of the neighboring atoms in different charge states. The most recent *ab initio* calculations[8] are also able to take into account the positron induced relaxation[4] and the ensuing positron lifetimes are in fair agreement with experiments. The association of the positron lifetime to the open volume of the defect has thus a solid theoretical basis.

However, the positron lifetime measurements give no information on the chemical surroundings of the annihilation event and cannot identify the sublattice of the vacancy or whether the vacancy is isolated or complexed with impurity atoms. Therefore, combining the lifetime measurements with a method giving additional information on the nearest-neighbor atoms of the defect would be of great value in the identification of point defects and defect complexes, especially in compound semiconductors.

In this paper we demonstrate the applicability of the Doppler broadening of the annihilation radiation[9] to the identification of defects in semiconductors. The Doppler broadening experiments provide information on the momentum distribution of the annihilating electrons.[9] One can easily distinguish between the low-momentum part of the spectrum, arising mainly from the annihilation with the valence electrons, and the higher-momentum parts coming from the core electrons. The umklapp annihilations contribute at high-momentum regions. Their amplitude, however, decreases with increasing momentum. The core electrons are tightly bound to the nuclei and thus the high-momentum parts of the Doppler spectrum carry information on the type of the atoms in the region scanned by the positron. In the case of open volume defects the positron wave function is localized and overlaps more strongly with the core electrons of the near-neighbor atoms than with those of the more distant atoms. In compound semiconductors, therefore, vacancies in different sublattices should give different signals to the Doppler spectrum. Moreover, impurity atoms associated to the vacancy may also be distinguished.

In the conventional single-detector Doppler technique the intensity of the high-momentum annihilation quanta is comparable to the background, which makes it difficult to make any conclusions on the shapes and magnitudes of the Doppler curve. To reduce the background we have used the coincidence measurement of both 511-keV γ rays in the Doppler experiment[10] which allows us to study the spectrum up to the momenta of 4.8 a.u., corresponding to the angle of 35 mrad between the two annihilation γ in an angular correlation experiment.

The rest of the paper is organized as follows. In Sec. II we describe the experimental setup used in the coincidence Doppler measurements. In Sec. III we present the theoretical background and describe a simple scheme to calculate the high-momentum parts of the Doppler spectrum. The method is demonstrated in Sec. IV by providing results for bulk Si, GaAs, and InP. As more specific examples of the defect applications, we have identified vacancies and vacancy-impurity complexes in InP. These results, as well as some problems related to this method, are discussed in Sec. V. Finally, we present our conclusions in Sec. VI.

II. EXPERIMENTAL METHOD

A. Experimental techniques

Positrons in a sample annihilate with electrons emitting two 511-keV γ rays. The 511-keV annihilation line is Doppler broadened due to the longitudinal momentum component, p_L of the annihilating electron-positron pair: $E_\gamma = (511 \pm \Delta E)$ keV. The Doppler shift $\Delta E = \frac{1}{2} p_L c$ is typically several keV, and it can thus be easily detected with a high-purity (HP) germanium γ-ray detector that has a resolution of 1.0–1.5 keV [full width at half maximum (FWHM)] at 511 keV. Because of the momentum conservation, the relative direction between the two emerging γ-rays deviates from 180° by a small angle, $\theta = p_T/m_0 c$ due to the transversal momentum component p_T. Both the Doppler broadening and one-dimensional angular correlation experiments (1D-ACAR), measure the equivalent momentum component denoted by p_z,

$$p_z = 2\Delta E/c = \theta_z m_0 c, \qquad (1)$$

where m_0 is the electron mass and c is the speed of light. Equation (1) implies that $\Delta E = 1$ keV in the Doppler experiments corresponds to $p_z = 0.54$ a.u. or $\theta_z = 3.91$ mrad in the 1D-ACAR experiments, if we define that the longitudinal momentum component is along z axis in Eq. (1).

As the resolution of the Ge detector is of the same order as the Doppler broadening, the details of the positron-electron momentum distribution are smeared out in the Doppler data as compared to the results of the ACAR experiments. Normally the Doppler spectrum suffers also from relatively high background radiation. If a ^{22}Na positron source is used, the background emerges mostly from the Compton scattering of the 1.28 MeV nuclear γ rays emitted together with the positron. The peak-to-background ratio of the Doppler spectrum is typically 100–200, which makes the detection of the high-momentum annihilation events difficult. Due to these limitations in the detection system, the Doppler results have been conventionally presented only in terms of integrated shape parameters, which describe the relative amounts of valence (S-parameter) and core (W-parameter) electron annihilations.

In order to study the high-momentum tails of the Doppler spectra, we have used a NaI detector in a coincidence with a HP Ge detector.[11] A ^{22}Na e^+ source is sandwiched between two pieces of the semiconductor sample. The Ge detector is used to detect the annihilation γ spectrum. The NaI scintillation detector is placed in collinear geometry with the Ge detector in order to detect the two 511-keV γ rays from the e^+-e^- annihilation. When pulses from both detectors arrive in coincidence, the pulse from the Ge detector is recorded in the memory of a multichannel analyzer (MCA). In this experiment the background is removed from the high-energy side of the 511-keV peak, but in the low-energy side the background largely remains due to the Compton scattering of the 511-keV γ rays. Compared to conventional Doppler

spectroscopy, the counting rate in the coincidence system is reduced only by the factor determined by the efficiency of the NaI detector. In our system the resolution of the Ge detector at 511-keV is 1.2 keV with 6-μs shaping time and 1.6 keV with 2-μs shaping time in the spectroscopy amplifier.

In the experimental setup described above, the coincidence rate n and the peak-to-background ratio p/b are related. When n decreases, p/b increases as the source-detector spacing d increases. We have used a positron source of 17 μCi and d=22 cm, which results to $n = 170$ 1/s in the 511-keV peak and $p/b = 2 \times 10^4$ on the high-energy side of the peak. In a typical experiment (1–4)$\times 10^7$ annihilation events were collected in the whole spectrum.

The Doppler spectrum suffers from pileup distortion, which is due to the piling up of the pulses especially in the preamplifier stage of the circuit. A pileup rejection signal is used to gate the MCA, but the remaining pileup effect can still be seen as a slowly decaying tail above 520 keV. The pileup effect is minimized by using a 2-μs shaping time in the spectroscopy amplifier. With this setup, the intensity of the pileup component is 2.3% of the core annihilation spectrum at ΔE=2.6–9.0 keV ($\theta_z = 10$–35 mrad), and the energy resolution of the system is 1.6 keV. In the final analysis the remaining pileup component is subtracted from the spectrum. We have also subtracted a constant background radiation from all the data. Figure 1 illustrates the difference between coincidence and conventional noncoincidence Doppler measurements. In coincidence measurements the background level is reduced by two orders of magnitude. The high-momentum tail arising from annihilations with core electrons is clearly observable at the energies above 515 keV.

After pileup and background subtraction the Doppler spectrum above 511-keV corresponds to the convoluted momentum distribution

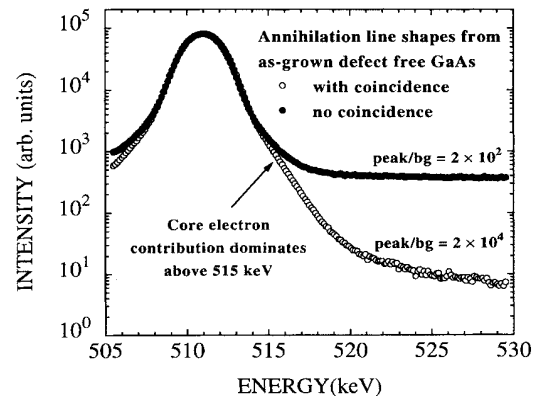$$f(\theta_z) = \Gamma(\theta_z) G(\theta_z), \qquad (2)$$

FIG. 1. Doppler broadened annihilation line shapes measured with the Ge detector. The figure shows the data obtained with and without the coincidence technique using a NaI detector in collision geometry with the Ge detector.

where $G(\theta_z)$ is the Gaussian resolution function of the Ge-detector, with FWHM=1.6 keV (6.2 mrad), and $\Gamma(\theta_z)$ is the integrated electron momentum distribution discussed further in Sec. III. Above 15 mrad the contribution from the valence electrons and the resolution function is negligible and thus $f(\theta_z) \approx \Gamma(\theta_z)$. The statistics in the spectra is sufficient up to 35 mrad. Therefore, comparisons between the experimental and theoretical core-electron momentum distributions can be done in the range of 15–35 mrad. In this comparison we present all the experimental data as a function of the angle θ_z calculated from Eq. (1).

B. Decomposition of the annihilation line

In practice the vacancy concentration in semiconductor crystals is often not large enough to induce complete positron trapping. In this case the Doppler spectrum has to be decomposed in order to obtain the annihilation line of positrons trapped at the vacancy defects. To achieve this the samples were studied with a conventional fast-fast lifetime spectrometer with a time resolution of 245 ps. A 10-μCi ^{22}Na source was sandwiched between two pieces of the sample and about 3×10^6 counts were collected in each spectrum. In the samples that contained vacancies a two component lifetime spectrum

$$n(t) = n_0(I_1 e^{-t/\tau_1} + I_2 e^{-t/\tau_2}) \qquad (3)$$

was fitted to determine the vacancy lifetime component $\tau_v = \tau_2$ and the average lifetime $\tau_{\text{ave}} = \sum_i I_i \tau_i$. The bulk lifetime τ_b is obtained from a sample in which there is no observed positron trapping.

In bulk samples the measured and corrected 511-keV annihilation line is straightforwardly the momentum distribution $f_b(\theta_z)$ of the electrons in the homogeneous bulk. In samples where the lifetime analysis indicates positron trapping at vacancies, both the bulk and vacancies contribute to the measured spectrum. If we assume only one type of defect, the measured distribution is a composition

$$f(\theta_z) = (1 - \eta_v)f_b(\theta_z) + \eta_v f_v(\theta_z), \qquad (4)$$

where $f_b(\theta_z)$ and $f_v(\theta_z)$ are annihilation lines in the bulk and at the vacancies, respectively, and η_v is the fraction of positron annihilating at the defect. Knowledge of $f_b(\theta_z)$ and η_v allows us to solve the equation for $f_v(\theta_z)$. Analogically, the average positron lifetime can be stated as

$$\tau_{\text{ave}} = (1 - \eta_v)\tau_b + \eta_v \tau_v. \qquad (5)$$

The positron lifetime measurements yield τ_{ave}, τ_b, and τ_v and the equation can be solved for η_v. Hence, the annihilation line for vacancies $f_v(\theta_z)$ can be extracted from Eq. (4).

The annihilation line at vacancies $f_v(\theta_z)$ is especially interesting in the high-momentum region ($\theta_z > 10$ mrad) where the core-electron contribution is dominant. At vacancies the high-momentum distribution reflects the chemical environment of the vacancy. Hence, the atoms surrounding the vacancy defect could be identified simply

from the *shape* of $f_v(\theta_z)$. On the other hand, the *magnitude* of the core-electron annihilation can be investigated using the W parameter

$$W = \frac{A_W}{A_{\text{tot}}}, \qquad (6)$$

where $A_W = \int_{\theta_1}^{\theta_2} f(\theta_z)d\theta_z$ and $A_{\text{tot}} = \int_0^{\infty} f(\theta_z)d\theta_z$ are areas of the measured Doppler curve. The boundaries θ_1 and θ_2 are chosen in such a way that W reflects mainly the core-electron annihilations in the system studied, and we have used the values $\theta_1 = 15$ mrad ($\Delta E = 3.8$ keV) and $\theta_2 = 20$ mrad ($\Delta E = 5.1$ keV). When differences in the shape of the core annihilation spectrum $f_v(\theta)$ are negligible, big changes may still be observed in the W parameter. Notice that the total area A_{tot} is calculated from one half of the peak starting from the centroid. This is due to our experimental system, in which the background is removed only from the high-energy side of the peak.

III. THEORY

The momentum distribution of the annihilating electron-positron pair can be written as

$$\rho(\mathbf{p}) = \pi r_0^2 c \sum_i \Big| \int d\mathbf{r} e^{i\mathbf{p} \cdot \mathbf{r}} \psi_i^{\text{ep}}(\mathbf{r}, \mathbf{r}) \Big|^2, \qquad (7)$$

where the summation is over all occupied electron states, $\mathbf{p}$ is the total momentum of the annihilating pair, and $\psi_i^{\text{ep}}(\mathbf{r}, \mathbf{r})$ is the two-particle wave function restricted to the case of the positron and electron residing at the same point. $\psi_i^{\text{ep}}(\mathbf{r}, \mathbf{r})$ can be approximated using the single-particle wave functions $\psi_+(\mathbf{r})$ and $\psi_-(\mathbf{r})$ for the positron and electron, respectively, and the enhancement factor $\gamma_i(\mathbf{r})$, taking into account the short-range electron pileup at the positron,

$$\psi_i^{\text{ep}}(\mathbf{r}, \mathbf{r}) = \psi_+(\mathbf{r})\psi_-(\mathbf{r})\sqrt{\gamma_i(\mathbf{r})}. \qquad (8)$$

In what follows, we shall make a simple approximation for both the electron and positron wave functions. Because we are mainly interested in the high-momentum part of the Doppler spectra, arising from the core electrons, we omit the contribution of the valence shells, taking the valence electrons into account at a later stage, through a proper normalization. This allows us to approximate the electron-core wave functions $\psi_i(\mathbf{r})$ by the ones obtained for free atoms. We use a nonrelativistic program,[15] based on density functional theory and the local density approximation (LDA), to calculate the wave functions for the core states. The positron wave function is also assumed to be spherical around each nucleus. In practice it is obtained by using the linear-muffin-tin-orbital (LMTO) method within the atomic-spheres approximation (ASA).[16] The positron potential corresponds to the self-consistent bulk electron structure and it is constructed (within the LDA) as a sum of Coulombic and correlation parts. We use the positron profiles

for bulk states also for atoms surrounding the vacancy defects. According to our LMTO-ASA–Green's-function calculations for the vacancy, the shape of the spherically averaged positron wave function around a neighboring atom differs only slightly from that in the perfect bulk. Therefore, this approximation does not appreciably affect the momentum distributions obtained as Fourier transforms. With these approximations we write the contribution of the n, l core state to the momentum distribution as

$$\rho_{nl}(p) = 4\pi \left| \int_0^\infty dr r^2 R_{nl}^-(r) R_{10}^+(r) j_l(pr) \right.$$
$$\left. \times \sqrt{\gamma(n_-(r))} \right|^2, \tag{9}$$

where $R_{nl}^-(r)$ and $R_{10}^+(r)$ are the radial parts of the electron and positron wave functions, respectively, and $j_l(pr)$ is the lth spherical Bessel function. Moreover, the enhancement factor $\gamma(n_-(r))$ is calculated from the total electron density $n_-(r)$ using the LDA[12,13] with the interpolation form suggested by Boroński and Nieminen.[14] The angular distribution, corresponding to the measured Doppler spectrum is obtained from Eq. (9) by integrating

$$\rho_{nl}(\theta_z) = \int_{p_z}^\infty dp p \rho_{nl}(p), \tag{10}$$

where $\theta_z = p_z/m_0 c$.

The contributions due to the different core states, calculated with Eq. (10) must be added together in order to get the total core part of the Doppler curve. In order to describe the solid in a realistic way, we have to find the proper weights for the contribution of each nl shell of each different atom type in a bulk or in a defected system. This can be done by calculating the corresponding partial positron annihilation rates. For this purpose we use the method of superimposed atoms[17] where the electron density and the Coulomb potential are obtained by superimposing free-atom densities and potentials. The total potential acting on the positron is the sum of the Coulombic potential and the correlation potential calculated in the LDA as in the case of our LMTO-ASA calculations. In the superimposed atom calculations we use a 64 atom supercell (63 in the case of vacancies). The electron density and the positron potential are calculated on a mesh with $32 \times 32 \times 32$ points forming a simple cubic lattice. The positron wave function is obtained by a relaxation method. A certain valence or core contribution to the annihilation rate is calculated as

$$\lambda^i = \int n_+(\mathbf{r}) \Gamma(n_-(\mathbf{r})) \frac{n^i(\mathbf{r})}{n_-(\mathbf{r})} d\mathbf{r}, \tag{11}$$

where $n^i(\mathbf{r})$ is the electron density contribution in question, $n_+(\mathbf{r}) = |\psi_+(\mathbf{r})|^2$ is the positron density, and $\Gamma(n_-(\mathbf{r}))$ is the annihilation rate in the LDA,[14] calculated using a correction due to the reduced screening in semiconductors.[18] Moreover, the positron lifetime τ is obtained as the inverse of the total annihilation rate $\lambda_{\rm tot}$

$$1/\tau = \lambda_{\rm tot} = \sum_i \lambda_i = \int n_+(\mathbf{r}) \Gamma(n_-(\mathbf{r})) d\mathbf{r}, \tag{12}$$

where the summation is over all different core and valence contributions.

The core contribution to the Doppler curve is obtained as

$$\rho(\theta_z) = \sum_i \lambda^i \rho_i(\theta_z), \tag{13}$$

where the index i runs over the core states. Above, in Eq. (13) the areas below the $\rho_i(\theta_z)$ curves are normalized to unity. Then the integral of the momentum distribution over θ_z gives the total core annihilation rate.

Finally, the theoretical counterpart of the experimental W parameter Eq. (7) is calculated as

$$W = \sum_i \lambda_i \left(\frac{A_W}{A_{\rm tot}} \right)_i / \lambda_{\rm tot}, \tag{14}$$

where $A_{\rm tot}$ is the total area of the angular distribution curve for core state i and A_W is the corresponding area in the W window, $\theta_1 \leq \theta_z \leq \theta_2$.

IV. RESULTS AND DISCUSSION

A. Core-electron momentum distribution in bulk semiconductors

To demonstrate the physics behind our method, and also to clarify the interpretation of the Doppler data, we first show results for bulk Si, GaAs, and InP. Figure 2(a) presents the experimental and Fig. 2(b) the calculated curves for these three semiconductors. In this and all the subsequent Doppler curves, the total areas under the curves are scaled to unity. In these figures, the effects of the dominant core shells are clearly seen. In GaAs, most of the core annihilation occurs with Ga and As $3d$ electrons, which are relatively tightly bound to the nuclei and quite localized in r space. Therefore, the corresponding momentum distribution is broad and extends to large momentum values. In InP, on the other hand, the dominant contribution to the core annihilation comes from In $4d$ electrons. They are less tightly bound, and extend to a wider region in r space and thus give a narrower and more rapidly descending contribution to the angular correlation curve. Since there are no d electrons in Si, and the annihilation is less likely to occur with Si $2s$ and $2p$ electrons because of the smaller screening of the nuclear Coulomb repulsion, the core part of the momentum distribution lies lower than it does in the case of GaAs and InP.

The contributions of the different core shells are demonstrated in Fig. 3, which presents the components $\lambda^i \rho_i(\theta_z)$ [see Eq. (13)] and the total curves of Fig. 2. In the case of InP [Fig. 3(a)] the dominant contribution up to 28 mrad comes from In $4d$. At very high momenta, P $2p$ gives the largest contribution. In GaAs [Fig. 3(b)], Ga $3d$ is seen to give more contribution than As $3d$, but the shape given by these dominant shells is very similar. In these figures, the contributions from P $3s$ and As $4s$

are also shown. These states are relatively low in energy. Being split off the valence bands they can have a remarkable contribution at relatively high momenta due to the ensuing spatial localization. As seen in Fig. 3(c), in the case of Si the annihilation with the 3s electrons is dominant at all except the very large momenta. This state is, however, valencelike and, therefore, it may be misleading to refer the corresponding annihilation rate as core annihilation. The inclusion of Si 3s to the total curve does not, however, change the qualitative picture of Fig. 2.

As can be seen in Fig. 2, much can be explained by the *shape* of the Doppler curves. It is also useful to analyze in a quantitative way the relative *amplitudes* of these curves. This is provided by the line-shape parameters S and W.[9] Here we concentrate on the W parameter, which is related to the core annihilation. Experimentally, the W parameter is the ratio of the area of some pre-defined window and the integral of the whole annihilation curve [Eq. (7)]. Due to the presence of background radiation at the larger momenta, this window is often defined around $10 - 15$ mrad. In this work the background level is much lower and we can thus determine the magnitude of the core-electron annihilation up to 30 mrad. Comparing the experimental curves of Fig. 2(a) and the theoretical ones of Fig. 2(b), it can be seen that all the experimental curves bend up with decreasing θ_z at values slightly larger than 10 mrad. This is due to the convolution by the broad energy resolution of the Ge γ detector system. The valence contribution, which is expected to die out well

below 10 mrad thus spreads to larger momenta, which makes it difficult to compare between experiment and theory, where only the core contribution is taken into account. We, therefore, prefer a W window that is 15–20 mrad. In this window the valence electron influence on the experimental curves is already negligible. In the following we will use only this W window.

For the reasons discussed in Sec. V, we compare only the relative W parameters, i.e., the ratios of W from two different systems, and not the absolute values. In Table I we show the ratios of the bulk W parameters, calculated from Fig. 2. The agreement between theory and experiment is seen to be fairly good. For comparison, the theoretical and experimental ratios $W^{\mathrm{InP}}/W^{\mathrm{Si}}$ are
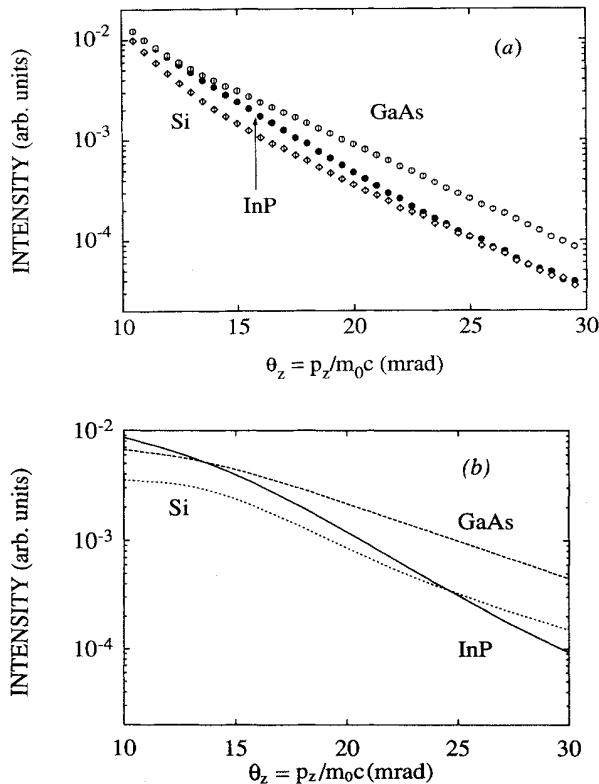

FIG. 2. High-momentum parts of the Doppler curves for bulk Si, GaAs, and InP; experimental (a), theoretical (b).
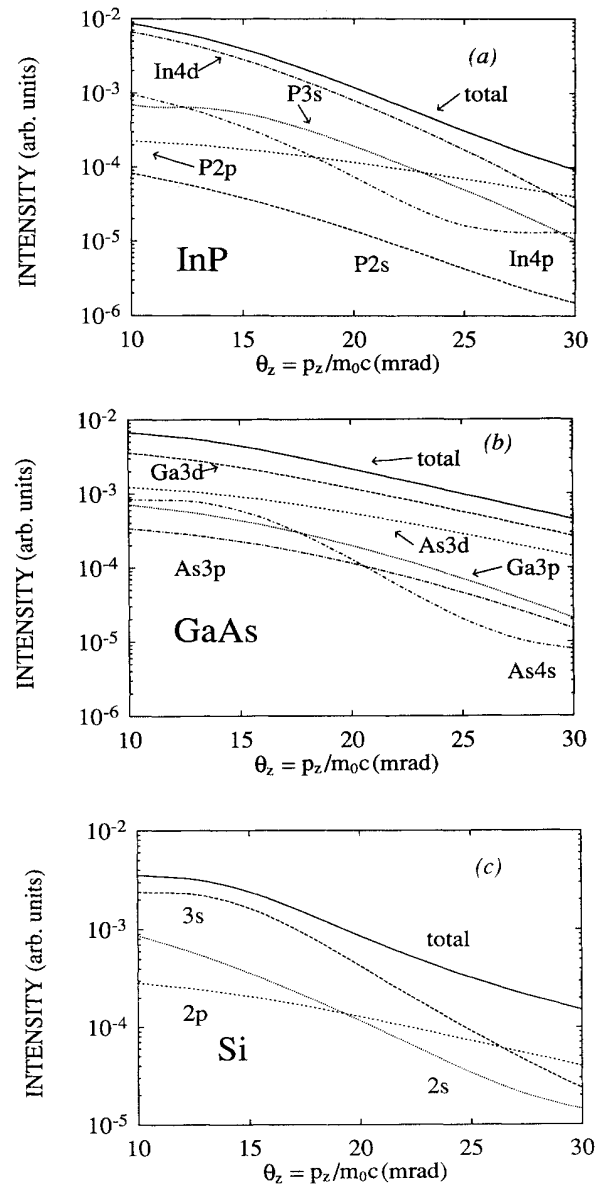
FIG. 3. Components of the angular correlation curves for (a) InP, (b) GaAs, and (c) Si.

TABLE I. Experimental and theoretical ratios (W/W_{Si}) of the bulk W parameters calculated using the window 15–20 mrad (514.8–516.1 keV).

System	Experiment	Theory
Si	1.00	1.00
GaAs	2.28	1.97
InP	1.54	1.44

1.86 and 1.37, respectively, when calculated in the usual 10–16 mrad window. This shows that the valence contribution distorts not only the shapes but also the relative amplitudes of the curves in that region.

The amplitudes of the bulk curves are related to the annihilation rates with different core shells. For bulk systems the most important contributions are shown in Table II (in the case of InP in Table III). In the case of GaAs and InP, most of the annihilation occurs with the d electrons, the annihilation rate with $3p$ electrons in GaAs and $4p$ electrons in InP is almost an order of magnitude smaller. As discussed above, the overall core annihilation rate in Si is small, and, therefore, the Doppler curve for Si lies lower than those for GaAs and InP, except for the region of very large momenta. Although these core annihilation rates give some hints about the trends the experimental W parameter shows between different systems, it can be concluded that a quantitative comparison of the theoretical results with the experimental ones requires the calculation of the weight factors $\left(\frac{A_W}{A_{tot}}\right)_i$ in Eq. (14).

B. Annihilation line shapes at elementary vacancies in InP

We now turn to the identification of the vacancies in our example case of InP. Positron lifetime experiments in electron irradiated InP have shown the creation of two different monovacancies depending on the conduction type of the samples.[19] After annealing at 300 K the vacancies present in semi-insulating Fe-doped InP give a positron lifetime of 283 ps whereas a positron trap with a lifetime 263 ps is observed in n-type S-doped InP. On the basis of the Fermi level position after irradiation, these vacancies have been identified as the In vacancy (283 ps) and the P vacancy (263 ps), respectively.

Figure 4(a) shows the experimental results for the va-

TABLE II. Annihilation rates λ_i (in ns^{-1}) for different core shells in bulk Si and GaAs.

Core shell	λ^i
Si 2s	0.034
Si 2p	0.106
Ga 3d	0.320·
Ga 3p	0.061
As 4s	0.577
As 3d	0.116
As 3p	0.030

TABLE III. Annihilation rates λ_i (in ns^{-1}) for different core shells in bulk InP, V_P, and V_{In}. V_P is relaxed outwards by 3% of the bulk bond length, V_{In} is assumed ideal.

	λ^i_{bulk}	$\lambda^i_{V_P}$	$\lambda^i_{V_{In}}$
In 4d	0.504	0.489	0.256
In 4p	0.077	0.071	0.037
P 3s	0.511	0.355	0.574
P 2p	0.022	0.014	0.019
P 2s	0.008	0.005	0.007

cancy defect found in electron irradiated InP(Fe) and InP(S), denoted V_{In} and V_P, respectively. The corresponding positron lifetimes are given in Table IV and they are in good agreement with the earlier values.[19] The curves in Fig. 4(a) indicate that the magnitude of the core-annihilation is much smaller in the vacancy in InP(Fe) than in bulk InP. However, the data in InP(S) are very close to the bulk curve, indicating a much larger amount of core-electron annihilations in the vacancy in InP(S) than in InP(Fe). This observation is in good agreement with the identification of vacancies in InP(Fe) with In vacancies and those in InP(S) with P vacancies. In the In vacancy the neighboring P atoms give only a small core-electron annihilation signal whereas in the P vacancy the positron annihilations with the core electrons of the surrounding In atoms yield almost as strong core
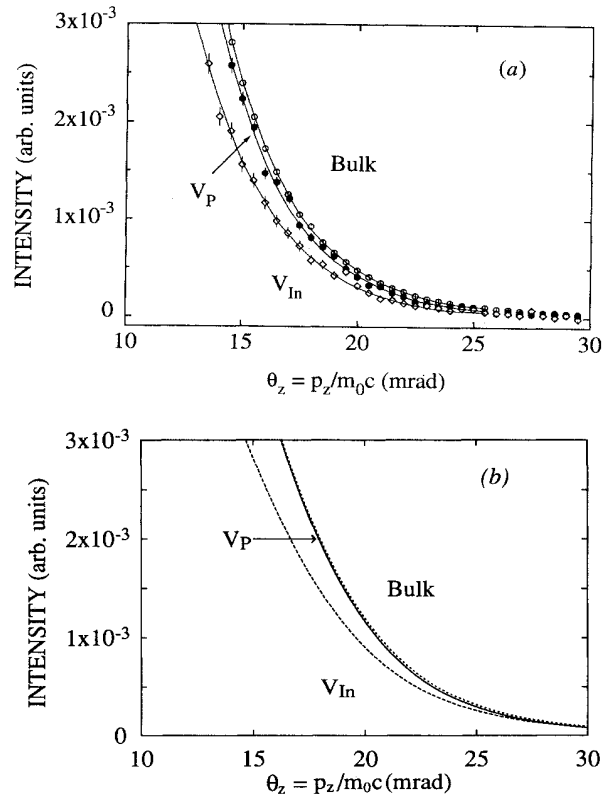

FIG. 4. High-momentum parts of the Doppler curves for bulk InP, phosphorous vacancy (V_P) and indium vacancy (V_{In}); experimental (a), theoretical (b). In (a) the lines are guides to the eye.

annihilation component as in the bulk. Hence, the magnitude of the core-electron annihilations can be used to identify the sublattice of the elementary vacancies in InP. However, the shape of the core annihilation line is almost similar for both In and P vacancies.

In the calculations, the lifetime for the ideal V_P is 255 ps, which is somewhat too short compared with the experimental one. This suggests a slight outward relaxation. We, therefore, calculated also the case where the four nearest-neighbor atoms of V_P were relaxed in the symmetric breathing mode outwards 3% of the bulk bond length. As seen in Tables IV and V, this gives a better resemblance to experiment both in the lifetime and in the W parameter. Relaxing another 3% outwards produces even better agreement in the W parameter, but the lifetime in that case is 8 ps too long. For V_{In}, the agreement is good already in the ideal case. These relaxations are in a slight disagreement with the ones calculated by Seitsonen *et al.*[6,7] showing typically an inward relaxation. The recent first principles calculations for GaAs by Gilgien *et al.*[8] show, however, that the positron induced relaxation is outwards. This relaxation, which was already discussed by Laasonen *et al.*,[4] can be of the order of 15% of the equilibrium bond length and, therefore, using the ideal (or nearly ideal) vacancies in our calculations is also justified from the calculational point of view.

The calculated core annihilation lines for In and P vacancies are shown in Fig. 4(b). The theoretical curves reproduce the trends seen in the experiments. The magnitude of the core-electron annihilations is much lower in V_{In} than in V_P. The curve obtained in the P vacancy is very close to that obtained in the bulk and the shapes of all these curves are very similar to each other. The good agreement of the theoretical and experimental data in Fig. 4 supports the identification of the vacancies in InP(Fe) and InP(S) to V_{In} and V_P, respectively. Furthermore, it demonstrates that the magnitude of the core-electron annihilations can be used to distinguish between vacancies at different sublattices in compound semiconductors like InP.

The calculated annihilation rates with individual core shells in both systems are shown in Table III. As expected, the dominant contribution in the case of V_P comes from In $4d$ electrons. All the other core states give annihilation rates that are an order of magnitude smaller than the one with In $4d$. Furthermore, the contributions of different shells presented in Fig. 5 show that In $4d$ is the dominant contribution also in the case of V_{In}. This might seem somewhat unexpected, because the nearest neighbors of V_{In} are P atoms, and the positron wave function is quite well localized, which means that the positron senses mostly the region where the dominant core contribution should come from P, most likely the P $2p$ elec-

TABLE IV. Experimental lifetimes τ (in ps) and W parameters relative to bulk (W/W_{bulk}) for bulk InP and vacancies.

System	τ	W/W_{bulk}
Bulk	244	1.00
V_{In}	283	0.70
V_P	267	0.94

TABLE V. Calculated lifetimes τ (in ps) and W parameters (W/W_{bulk}) for bulk InP and vacancies. The percentages taken relative to the bulk bond length, refer to the amount of outward breathing mode relaxation.

System	τ	W/W_{bulk}
Bulk	240	1.00
V_{In} (ideal)	280	0.73
V_P (ideal)	255	1.01
V_P (3%)	264	0.98
V_P (6%)	275	0.95

trons. These electrons, however, are localized in a region close to the nucleus, where the Coulomb repulsion affecting the positron is so large that it prevents the positron from penetrating into the P $2p$ shell. Thus the overlap of the positron wave function with the $4d$ electrons of the next-nearest-neighbor In atoms is enough to give a larger annihilation rate than that with P $2p$ electrons. As seen in Table III, the total core annihilation rate for V_{In} is smaller than for V_P. This is reflected also in the W parameters. Tables IV and V give the defect W parameters relative to the bulk W for both vacancy types. Again, the agreement between theory and experiment is fairly good. This supports again our calculations also as a quantitatively predictive method.
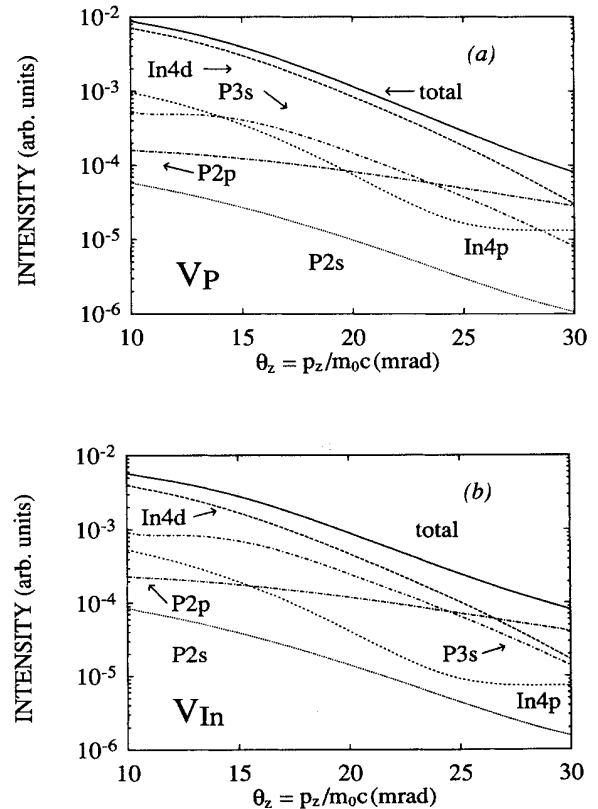

FIG. 5. Components of the angular correlation curves for (a) phosphorous vacancy (V_P) and (b) indium vacancy (V_{In}).

C. Impurity-vacancy complexes: Zn in InP

A very interesting application is the identification of vacancy-impurity complexes. The decoration of a vacancy by impurities normally does not change the positron lifetime considerably. However, if the electronic structure of the impurity differs significantly from that of the host atoms, the impurity in the vicinity of the vacancy may be distinguished simply from the shape of the core-electron annihilation line.

Heavily Zn-doped InP has been found to contain native vacancy defects with a positron lifetime of about 325 ps.[20] We have studied this type of sample with a Zn concentration of 6.4×10^{18} cm^{-3} and obtained similar positron lifetime results as earlier.[20] Figure 6 presents the experimental Doppler curve for this sample. The corresponding curve for a sample containing P vacancies is shown for comparison. The shape of the curve for the Zn-doped sample is broader than those for V_{In} and V_P. This indicates that the native vacancy observed in InP(Zn) is different from both isolated In and P vacancies. As explained in the case of bulk data in Sec. IV A (Fig. 2), $3d$ electrons give a broader distribution than $4d$ electrons. The broad high-momentum part can thus be associated with the $3d$ electrons of Zn atoms surrounding the vacancy. Although the lifetime at the vacancy is large (325 ps), the curve in InP(Zn) lies high at all momenta, indicating a large magnitude of core-electron annihilations. As shown in Sec. IV B, this effect is the fingerprint of the phosphorous vacancy. We can thus identify the native vacancy observed in InP(Zn) with the P vacancy decorated by Zn impurities.

We have performed model calculations of positron lifetimes and core annihilation lines for various defect complexes involving V_P and Zn. The calculated lifetimes and W parameters for some of these complexes are shown in Table VI. As seen in the table, a breathing mode relaxation of 17% is needed to produce a lifetime that is close to the experimental value when one Zn atom is placed to the neighborhood of the vacancy. In this configuration the shape of the core annihilation line is very similar to the experimental curve, but the W parameter is slightly smaller than the experimental one. The quantitative agreement becomes even better by replacing two of the nearest-neighbor In atoms of the P vacancy by Zn. This system has to be relaxed outwards by 14% in order to get a lifetime near the experimental one. In this case also the W parameter is in close resemblance with the experiment (Table VI). The calculated core annihilation

line for this configuration [Fig. 6(b)] shows clearly the broadening induced by Zn atoms neighboring V_P, and it is in good agreement with the experimental curve [Fig. 6(a)].

Finally, we have studied the configuration suggested by Tuck and Hooper,[21] where there is a Zn atom at an In site between two P vacancies, denoted by $V_P Zn_{In} V_P$. Our calculated (assuming ideal lattice positions) lifetime for this complex, 327 ps, agrees well with the experimental one. The calculated relative W parameter, however, is 0.74, which differs clearly from the experimental value of 1.05.

To conclude the results of the model calculations, the replacement of the nearest-neighbor In atoms of the P vacancy by Zn changes the core annihilation line in a way similar to that seen in the experiments. The theory is also able to reproduce the long lifetime of 325 ps and the relatively high W-parameter value due to the decoration of P vacancy by Zn atoms. We can thus conclude that the calculations support the identification of the native vacancy in InP(Zn) with a phosphorous vacancy surrounded by Zn impurities.
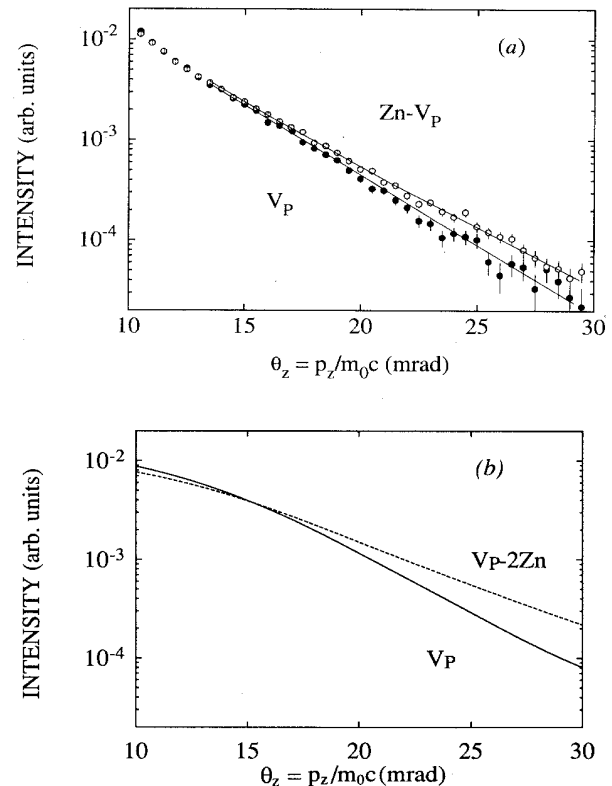

TABLE VI. Lifetimes τ (in ps) and W parameters (W/W_{bulk}) for different V_P-Zn complexes.

	τ	W/W_{bulk}
Experiment	325	1.05
Theory		
V_P (19%)	323	0.75
V_P-Zn (ideal)	264	1.14
V_P-Zn (17%)	322	0.91
V_P-2Zn (14%)	319	1.08
V_P-Zn$_{In}$ - V_P	327	0.74

FIG. 6. (a) Measured Doppler curves for a sample containing phosphorous vacancies (V_P) and for a highly Zn-doped sample (V_P-Zn). The lines are guides to the eye. (b) Calculated Doppler curves for a phosphorous vacancy in InP, relaxed 3% of the bulk bond length outwards in the breathing mode and a phosphorous vacancy, decorated with two Zn atoms and relaxed 14% of the bulk bond length outwards in the breathing mode.

V. SUMMARY AND COMPARISON BETWEEN THEORY AND EXPERIMENT

The measured Doppler curves can be interpreted by analyzing their shapes and amplitudes. On the other hand, the experimental line shapes can be reproduced reasonably well by the simple calculations. The differences in the shapes are due to the different cores of the constituent atoms; for example even the two d shells, $3d$ and $4d$ give remarkably different line shapes.

In compounds like InP, where the constituents have clearly different core sizes (In has d-electrons whereas P has not) our method yields big differences in the magnitude of the core annihilation at vacancies in different sublattices. The sublattice of the vacancy can thus be simply distinguished by the magnitude of the core annihilation using the W parameters. However, the annihilation line shapes are very similar because P atoms give essentially no signal. In the case of GaAs, for example, where the ionic cores have the same population of electrons, it is more difficult to distinguish between the vacancies in different sublattices by the shape of the momentum distribution. However, the nuclear charge is even in this case different, and it may cause a tractable effect to the amplitude of the momentum distribution of the core-electrons. Moreover, as we have demonstrated for V_P-Zn in InP, the identification of vacancy-impurity pairs should also be possible in these compounds as well as in elemental semiconductors such as Si and Ge.

When comparing quantitatively theory with experiment, the relevant quantities to consider are the relative values of the W parameters and not the absolute ones. For example, in the case of bulk InP and GaAs, the calculated absolute W parameters are larger than the experimental ones by a factor of 2. This can be traced back mainly to the enhancement factor used in calculating the angular correlations of the individual core shells. We have estimated for bulk InP the momentum dependence of the Boroński-Nieminen enhancement factor[14] using the definition of Bonderup, Andersen, and Lowy,[22]

$$\gamma(\mathbf{p}) = \rho^{\mathrm{LDA}}(\mathbf{p})/\rho^{\mathrm{IPM}}(\mathbf{p}), \qquad (15)$$

where $\rho^{\mathrm{LDA}}(\mathbf{p})$ is the momentum distribution calculated

with the LDA enhancement factor and $\rho^{\mathrm{IPM}}(\mathbf{p})$ is the momentum distribution calculated within the independent particle model (IPM), i.e., neglecting the enhancement by setting $\gamma(n_-(r)) = 0$. It turns out that the enhancement is almost independent of the momentum. It decreases from a value close to 3 to 2 when the θ_z increases from 10 mrad to 30 mrad, whereas the comparison of the present measurement with the IPM calculation indicates that the enhancement should be close to unity in the region $\theta_z > 20$ mrad. Furthermore, the ratios $W^{\mathrm{def}}/W^{\mathrm{bulk}}$ of the W parameters are less sensitive to the approximations in the calculations because the same angular distributions $\rho_i(\theta_z)$ are used for bulk and defected systems, only with different weights.

VI. CONCLUSIONS

We have used Doppler broadening of positron-electron annihilation radiation to identify vacancies in compound semiconductors. Coincidence detection of the annihilation quanta was used to decrease the experimental background in order to extract the core-electron signal. We further present a simple calculation scheme to obtain the core-electron annihilation line. It is concluded that the Doppler experiment can be used to identify the sublattices of the vacancy and the association of the vacancy with impurity atoms. The Doppler technique is thus shown to yield complementary information to the positron lifetime results in defect identification. The comparison of the theoretical results with the experimental ones is essential in reaching this goal.

In this work, we have applied the Doppler broadening technique to identify vacancy defects in InP. In electron irradiated InP vacancy defects with a positron lifetimes of 283 ps and 263 ps are identified as In and P vacancies, respectively. We have also studied native vacancies in heavily Zn-doped InP. In the annihilation line at the vacancy the contribution of the Zn $3d$ electrons was observed in addition to that of In $4d$. Furthermore, the long positron lifetime of 325 ps at this defect is accompanied by a large magnitude of core-electron annihilations. On the basis of this information we identify this native defect with a phosphorous vacancy decorated by Zn atoms.

[1] For reviews see, P. Hautojärvi and C. Corbel (unpublished); M. J. Puska, Phys. Status Solidi A **102**, 11 (1987), and references therein; M. J. Puska and R. M. Nieminen, Rev. Mod. Phys. **66**, 841 (1994).

[2] M. J. Puska and C. Corbel, Phys. Rev. B **38**, 9874 (1988).

[3] K. Saarinen, P. Hautojärvi, P. Lanki, and C. Corbel, Phys. Rev. B **44**, 10 585 (1991); C. Corbel, M. Stucky, P. Hautojärvi, K. Saarinen, and P. Moser, *ibid.* **38**, 8192 (1988); J. Mäkinen, P. Hautojärvi, and C. Corbel, J. Phys. Condens. Matter **4**, 5137 (1992).

[4] K. Laasonen, M. Alatalo, M. J. Puska, and R. M. Nieminen, J. Phys. Condens. Matter **3**, 7217 (1991).

[5] K. Laasonen, M. J. Puska, and R. M. Nieminen, Phys. Rev. B **45**, 4122 (1992).

[6] M. Alatalo, R. M. Nieminen, M. J. Puska, A. P. Seitsonen, and R. Virkkunen, Phys. Rev. B **47**, 6381 (1993).

[7] A. P. Seitsonen, R. Virkkunen, M. J. Puska, and R. M. Nieminen, Phys. Rev. B **49**, 5253 (1994).

[8] L. Gilgien, G. Galli, F. Gygi, and R. Car, Phys. Rev. Lett. **72**, 3214 (1994).

[9] *Positrons in Solids*, edited by P. Hautojärvi, Topics in Current Physics Vol. 12 (Springer-Verlag, Heidelberg, 1979).

[10] K. G. Lynn, J. R. MacDonald, R. A. Boie, L. C. Feldman, J. D. Gabbe, M. F. Robbins, E. Bonderup, and J. Golovchenko, Phys. Rev. Lett. **38**, 241 (1977); K. G. Lynn, J. E. Dickman, W. L. Brown, M. F. Robbins, and E. Bonderup, Phys. Rev. B **20**, 3566 (1979).

[11] K. G. Lynn and A. N. Goland, Solid State Commun. **18**,

1549 (1976).

[12] S. Daniuk, G. Kontrym-Sznajd, A. Rubaszek, H. Stachowiak, J. Mayers, P. A. Walters, and R. N. West, J. Phys. F **17**, 1365 (1987).

[13] T. Jarlborg and A. K. Singh, Phys. Rev. B **36**, 4660 (1987).

[14] E. Boroński and R. M. Nieminen, Phys. Rev. B **34**, 3280 (1986); J. Arponen and E. Pajanne, Ann. Phys. (N.Y.) **121**, 343 (1979).

[15] A. Zangwill and D. A. Liberman, Comp. Phys. Comm. **32**, 63 (1977).

[16] H. C. Skriver, *The LMTO Method* (Springer, New York, 1984). For the applications of the LMTO method to positron states, see A. K. Singh and T. Jarlborg, J. Phys. F **15**, 727 (1985); M. J. Puska, O. Jepsen, O. Gunnarson,

and R. M. Nieminen, Phys. Rev. B **34**, 2695 (1986).

[17] M. J. Puska and R. M. Nieminen, J. Phys. F **13**, 2695 (1983).

[18] M. J. Puska, S. Mäkinen, M. Manninen, and R. M. Nieminen, Phys. Rev. B **39**, 7666 (1989).

[19] M. Törnqvist, J. Nissilä, F. Kiessling, C. Corbel, K. Saarinen, A. P. Seitsonen, and P. Hautojärvi, Mater. Sci. Forum **143-147**, 347 (1994).

[20] G. Dlubek, O. Brümmer, F. Plazaola, P. Hautojärvi, and K. Naukkarinen, Appl. Phys. Lett. **46**, 1136 (1985).

[21] B. Tuck and A. Hooper, J. Phys. D **8**, 1806 (1975).

[22] E. Bonderup, J. U. Andersen, and D. N. Lowy, Phys. Rev. B **20**, 883 (1979).